Study of Gas-Solid Slugging Fluidized Bed with Geldart D Particles Using High-Temperature Electrical Capacitance Volume Tomography

THESIS

Presented in Partial Fulfillment of the Requirements for the Degree Master of Science in the Graduate School of The Ohio State University

By

Mingyuan Xu

Graduate Program in Chemical and Biomolecular Engineering

The Ohio State University

2017

Master's Examination Committee:

Professor Liang-Shih Fan, Advisor

Professor Jeffrey Chalmers

Abstract

Electrical capacitance volume tomography (ECVT) is a novel 3-D imaging technology for multiphase flow systems. It can capture dynamic flow behaviors in real time and with sufficient fidelity, which can be useful for laboratory fluid mechanics studies as well as industrial process monitoring and diagnosis. To date, ECVT has been successfully applied to various multiphase flow systems, including gas-solid fluidized bed, gas-liquid bubbling bed, gas-solid-liquid trickle bed and flow systems with complex geometries. However, since ECVT was initially developed only for cold flow systems, most of the experiments are conducted at ambient temperature. High-temperature applications of ECVT are greatly desired since most industrial processes operate at elevated temperatures. For example, it is proposed to use ECVT for imaging solid flow at 1000 °C in chemical looping systems to provide real time solids circulation data. To explore the possibilities of employing ECVT at high temperatures, a special heated fluidized bed test unit is built with ceramic inner lining in the ECVT sensor assembly, which protects the sensor from excess heat at high temperatures.

Work in this thesis is focused on studying the slugging phenomenon at different temperatures in the fluidized bed test unit with Geldart D chemical looping oxygen carrier particles as the fluidized solid and air as the fluidizing gas. It not only serves to evaluate the performance of ECVT at high temperatures, but also to examine the effect of

temperature on slugging fluidized bed behaviors. Little research has been published on this topic due to the difficulty of fluidized bed characterizations at high temperatures. The experiments were conducted at temperatures ranging from 25 °C to above 700 °C. The results show that slug rise velocity and frequency increase as gas velocity increases, which is consistent with literature data and theory. The results also show that the effect of temperature on the correlation between gas velocity and slug properties is minimal. In addition, a preliminary test for solids circulation rate measurement is conducted in the test unit to explore the proposed application of ECVT in chemical looping. Future plans for the test unit and continuing research on the slugging behavior are also proposed.

Dedication

To my family and friends

Acknowledgments

I would like to extend my deepest appreciation to my advisor, Dr. Liang-Shih Fan, for giving me the opportunity to work on multiple exciting research projects and be a part of his amazing research group. Dr. Fan's enthusiasm, diligence and devotion for research will be an inspiration for me forever.

I am sincerely thankful to Dr. Andrew Tong for giving me tremendous help and guidance every step along the way, and for managing the many projects in the group.

I am truly grateful to Dr. Jeffrey Chalmers for joining my Master's examination committee, and for giving me a memorable TA experience.

I would like to thank all the former and current members of my research group. Particularly, I would like to thank Dr. Dawei Wang and Dr. Pengfei He for their tremendous contribution to the ECVT project, Dr. Aining Wang for introducing me to ECVT, Yaswanth Pottimurthy, Cody Park and Marshall Pickarts for their help with the ECVT experiments. I would like to thank Dr. Alan Wang for his guidance through my initial research experience. I would like to thank Dikai Xu, Tien-Lin Hsieh and Cheng Chung for their support and advice. I would like to thank Mengqing Guo, Yitao Zhang, Sourabh Nadgouda,

Fanhe Kong, Yu-Yen Chen, Deven Baser, Prateek Kumar, Yan Liu, Chenghao Wang and Vedant Shah for their help and support. I would like to thank Dr. Lang Qin, Dr. Zhuo Cheng and Dr. Mandar Kathe for their guidance and support.

I would thank everyone who helped me in various ways, especially Dr. Qussai Marashdeh and Benjamin Straiton from Tech4Imaging for their support on the ECVT project, Mr. Michael Wilson and Mr. Leigh Evrard for their help with the projects, and Ms. Lynn Flanagan, Ms. Susan Tesfai, and Ms. Angela Bennett for their administrative help and support.

Finally, I would like to thank my parents for their endless love and support.

Vita

December 19, 1992 .....Born – Luoyang, Henan, China

August 2011 – July 2015 .....B.Eng. Chemical Engineering, B.A. Art,
Tsinghua University, Beijing, China

August 2015 – present .....Graduate Research Associate,
The Ohio State University

Publications

Qin, L.; Guo, M.; Cheng, Z.; **Xu, M.**; Liu, Y.; Xu, D.; Fan, J. A.; Fan, L.-S., Improved cyclic redox reactivity of lanthanum modified iron-based oxygen carriers in carbon monoxide chemical looping combustion. *J. Mater. Chem. A* **2017**.

Qin, L.; Cheng, Z.; Guo, M.; **Xu, M.**; Fan, J. A.; Fan, L.-S., Impact of 1% Lanthanum Dopant on Carbonaceous Fuel Redox Reactions with an Iron-Based Oxygen Carrier in Chemical Looping Processes. *ACS Energy Letters* **2017**, 2 (1), 70-74.

Cheng, Z.; Qin, L.; Guo, M.; **Xu, M.**; Fan, J. A.; Fan, L. S., Oxygen vacancy promoted methane partial oxidation over iron oxide oxygen carriers in the chemical looping process. *Phys Chem Chem Phys* **2016**, 18 (47), 32418-32428.

Fields of Study

Major Field: Chemical and Biomolecular Engineering

Table of Contents

List of Figures

Chapter 1: Introduction

Electrical capacitance volume tomography (ECVT) is a novel low-cost, non-intrusive 3-D imaging technology that is capable of visualizing multiphase flow systems under various conditions in real-time. In the past decade, ECVT technology has been developed and implemented at The Ohio State University to study gas-solid, gas-liquid and gas-solid-liquid flow systems in corporation with Tech4Imaging[1]. Recently, a high-temperature fluidized bed reactor with customized ECVT sensor is built at The Ohio State University to study gas-solid system behaviors as well as to evaluate the performance of ECVT at elevated temperatures. A potential application of the high-temperature ECVT technology is the solids circulation rate measurement for the advanced control and automation of the moving-bed chemical looping systems developed at The Ohio State University.

In Chapter 1, a brief introduction of the chemical looping technology is presented. The motivation for developing high-temperature ECVT for moving-bed chemical looping systems is explained. Then the principles of ECVT is briefly introduced, and examples of various applications of ECVT are presented. In the end, a summary of the past studies on the slugging behavior in gas-solid fluidized bed systems is offered.

In Chapter 2, the design and setup of the newly-built high-temperature ECVT apparatus is described in detail. The experimental design and procedures for slugging fluidized bed characterizations are also explained.

In Chapter 3, the experimental results are presented, which include the reconstructed images of the slugging fluidized bed and the slug velocity and frequency measurements obtained from the images at different gas flow rates and temperatures. The correlations between slug velocity/frequency and gas flow rate are established, and are compared with literate data. The effect of high temperature on the correlations is found to be minimal. In the end, the conclusion on the performance ECVT at high temperatures is drawn and future plans for continuing slugging fluidized bed studies and exploring applications of ECVT in chemical looping systems are discussed.

1.1 Chemical Looping Systems

1.1.1 CO_2 Emission and Carbon Capture

As the world population continues to increase and global economy continues to grow, the world energy demand is expected to increase by 48 % from the year 2012 to 2040[2]. Although renewable energy has seen a rapid growth in recent years, traditional fossil fuels will remain to be the dominating source of the world energy supply, and will account for 78 % of the total energy use in 2040[2]. The enormous amount of CO_2 generated every year from the consumption of carbonaceous fossil fuels has caused major concerns and heated debates over its crucial role in global warming and climate change due to its greenhouse

effect. In response, a number of countries have made efforts to regulate CO_2 emissions, including the United States, whom, accounting for 15 % of global CO_2 emission in 2012, is the second largest producer of CO_2 after China[2]. Among fossil fuels, coal and natural gas, which are both commonly used for electricity generation, together account for about 60 % of global CO_2 emissions and will remain on the same level until 2040[2]. In the United States, about 40 % of CO_2 emissions in 2011 is from power generation[3]. Although this number is slowly decreasing as coal-fired power plants are gradually replaced with cleaner natural gas-based plants and renewable energy sources, coal and natural gas-based power plants will remain to be the main source of electricity[3]. Thus, low-cost carbon capture technologies that can substitute or be retrofitted to existing power plants and are still highly desired to effectively reduce CO_2 emissions.

Carbon capture and storage (CCS) is currently the most intensely researched topic on CO_2 emission mitigation. Several of its technologies have already being implemented, or are under comprehensive research and development. CCS can be further divided into CO_2 capture, transport and storage. As for transport, pipeline-based and vehicle-based methods have been demonstrated at industrial scale. For storage, geological sequestration of CO_2 is believed to be feasible, and other alternatives, including mineral carbonation and CO_2 utilization are being actively investigated. However, compared to these two aspects, CO_2 capture requires significantly more development costs and faces more economical and engineering challenges[4]. Carbon capture technologies are often categorized into post-combustion capture, pre-combustion capture, oxy-combustion, direct air capture and chemical looping combustion[5]. In post-combustion, solvents, sorbents, solids or

membranes are used to absorb or separate CO_2 from flue gas, but the energy penalty is high because of the low CO_2 concentration in the flue gas[6]. In pre-combustion, coal is gasified to produce syngas, which is further converted to CO_2 and hydrogen (H_2) though water-gas shift reaction. This mixture is easier for carbon capture because of higher CO_2 concentration, and the H_2 stream after CO_2 separation is used for power generation. However, the cost of the gasification process is high. Oxy-combustion uses pure oxygen instead of air to burn fuel, which generates a flue gas stream with high CO_2 concentration that is sufficient for carbon storage, but the auxiliary air separation unit for oxygen generation is costly[7]. Direct air capture aims at collecting CO_2 from the atmosphere and generate concentrated CO_2 stream using physical and chemical processes. This technology is still largely under laboratory development and the cost is expected to be the highest among all CCS technologies[5].

1.1.2 Chemical Looping Technology

Chemical looping combustion uses metal-oxide based solid-state oxygen carriers to react with carbonaceous fuels in the fuel reactor called reducer, which produces pure CO_2 as the only gaseous species that is inherently separated from the other solid species. The reduced oxygen carriers are combusted in the air reactor called combustor to regenerate and are then recycled back to the reducer. Chemical looping is promising due to its economic feasibility. Compared to the technologies mentioned above, the inherent CO_2 separation in chemical looping avoids any energy and capital-intensive gas separation process and provides significant cost savings[8]. Conventional design of a chemical looping system

involves two to three interconnected fluidized beds. The Ohio State chemical looping technology applies the moving-bed concept in the reducer, which achieves a higher oxygen carrier conversion compared to the fluidized bed design[9]. Ohio State has demonstrated sub-pilot scale chemical looping systems with several types of fuel as input, including syngas, methane, biomass and coal[8], and the development of the moving-bed chemical looping technology at Ohio State is summarized in the following figure:

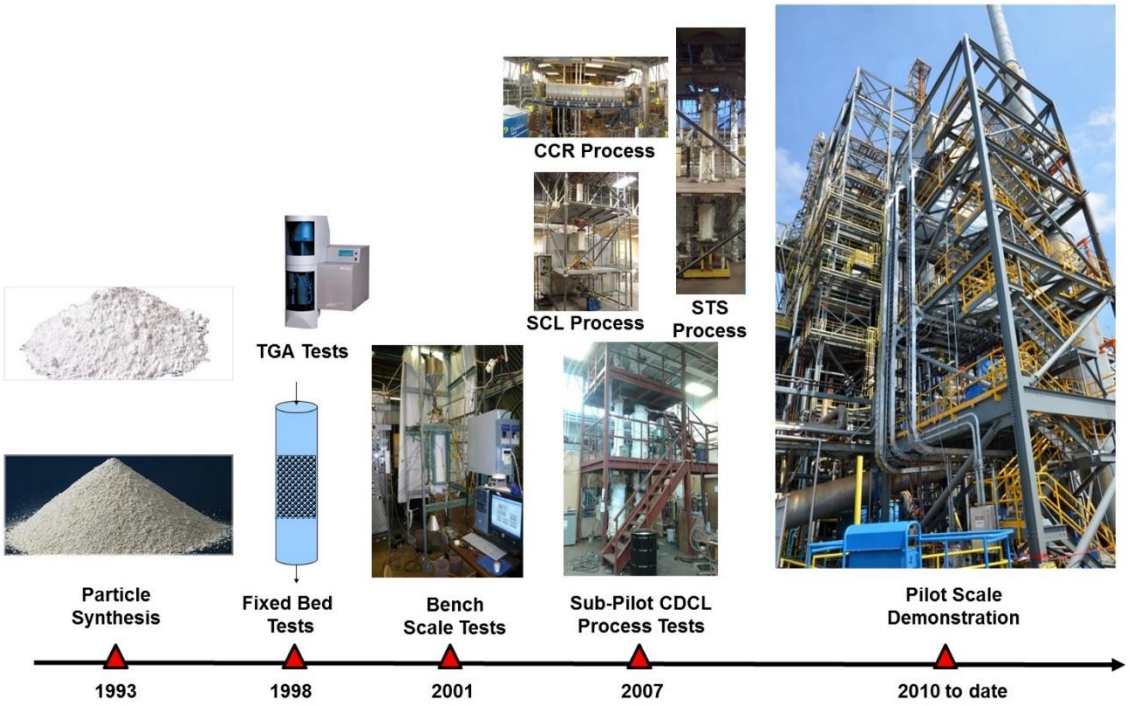

Figure 1. Roadmap of the development of the moving-bed chemical looping technology at The Ohio State University[10].

Currently there are several ongoing projects at Ohio State for developing the moving-bed chemical looping technology, which span from economic analysis, novel process design and testing to chemical looping plant scale-up. One of the project aims to achieve fully automatic control of chemical looping systems, including automatic start up, shut down and normal operation. To achieve automatic control, a number of process variables have to be recorded in real time in an operation to be sent to the control program for decision making. Common process variables such as temperature and pressure can be obtained using existing process instruments. One process variable that is unique to the moving-bed chemical looping system is the solids circulation rate. The ratio between the oxygen carrier solids circulation rate and the inlet fuel flow rate dictates the fuel and solids conversion, which are both crucial to the performance of the plant. An illustration of the effect of oxygen carrier to fuel ratio on the conversions is shown as follows:

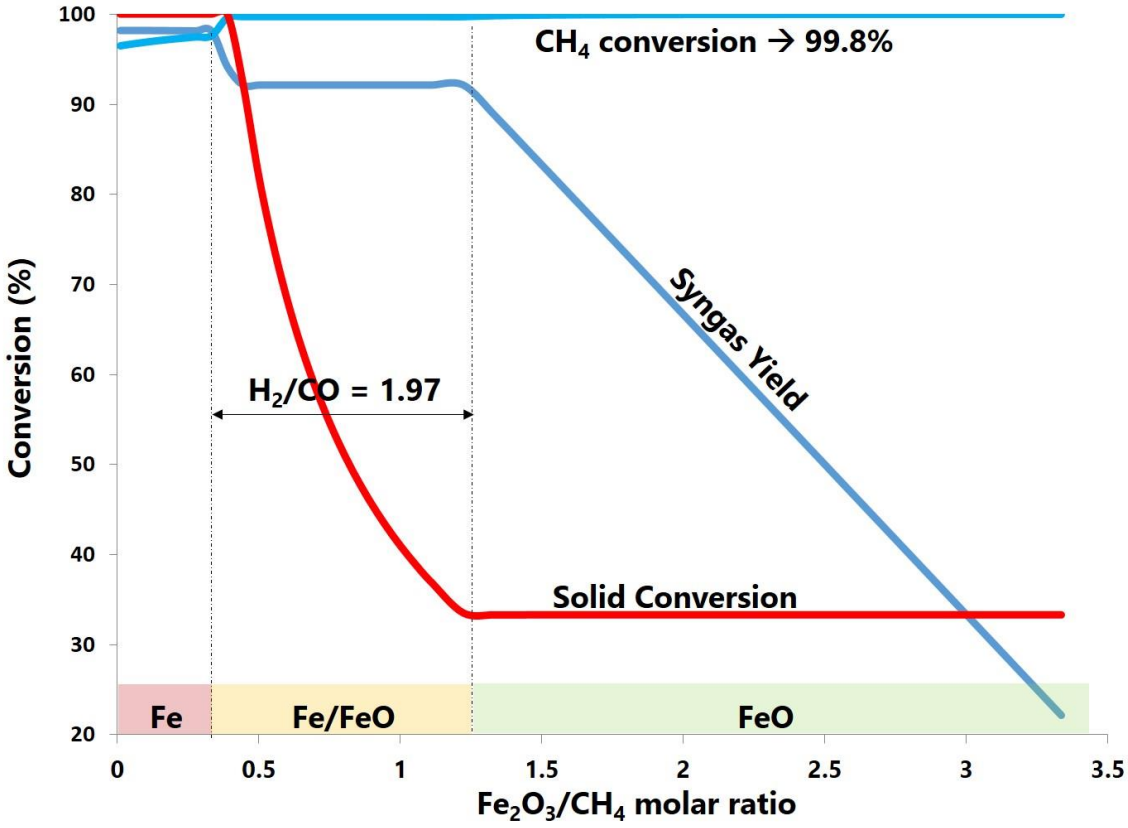

Figure 2. Impact of oxygen carrier (Fe_2O_3)to fuel (CH_4) ratio on oxygen carrier and fuel conversions in the chemical looping methane to syngas (MTS) process[11].

It can be seen that in the MTS process, only when the solids to fuel ratio is maintained between 0.4 and 1.4 can the syngas ratio, yield and purity be optimal. However, the solids circulation rate is often hard to measure. Only a few working methods exist, including temperature signal correlation, where the solids moving velocity is deduced from the change in the temperature profile along the moving bed caused by the passing of a cluster of cold solids; isokinetic measurement, where a small pipe filled with solids is inserted into the moving bed and the solids velocity in the moving bed can be deduced from the solids velocity in the pipe; and cold flow model study, where a cold flow model of chemical looping system is built and the relationship between the solids circulation rate and the aeration gas is established. However, none of these methods can provide accurate solids circulation rate in real time, which is a crucial prerequisite for automatic control systems. ECVT can potentially be used to measure solids flow rate in a chemical looping system, either at the standpipe with downward packed bed flow, where the motion of irregularities in the solids can be captured by ECVT and translated to solids velocity, or at the riser with upward slugging flow, where periodic solids slugs can be recorded by ECVT and translated to solids flow rate. An illustration of the existing and proposed methods for solids circulation rate measurement is shown as follows:

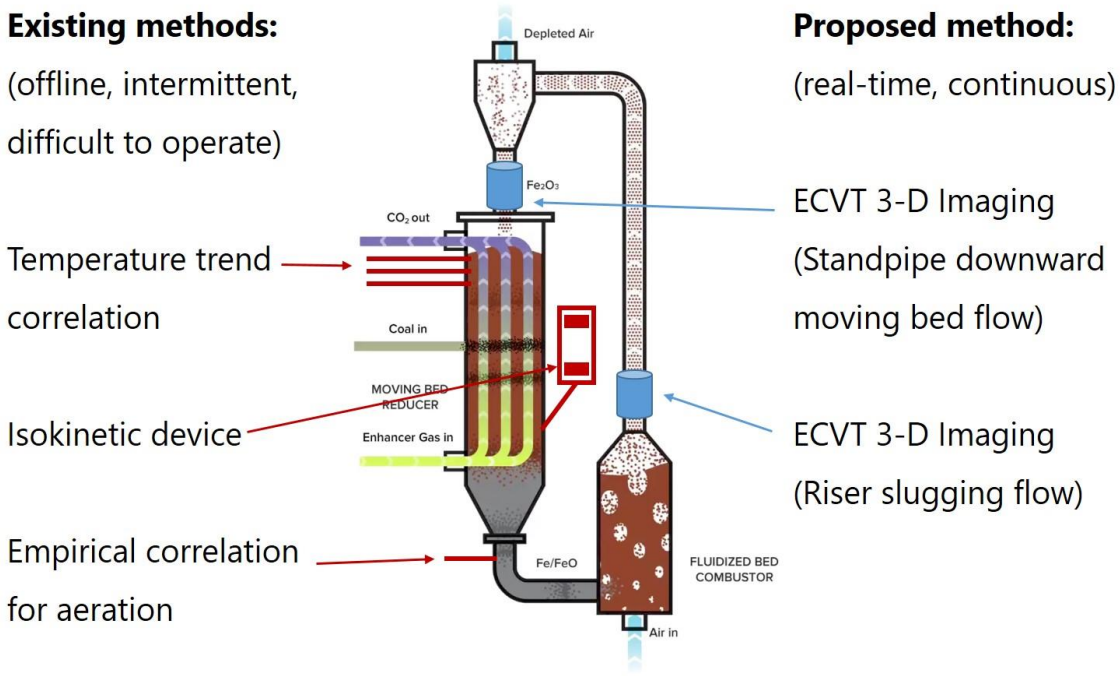

Figure 3. Current and proposed methods for measuring solids circulation rate in a moving-bed chemical looping system.

1.2 Electrical Capacitance Volume Tomography (ECVT)

1.2.1 Principles of ECVT

ECVT is a non-invasive 3-D tomography technology that can be used for imaging gas-solid and gas-liquid flow systems. It is derived from electrical capacitance tomography (ECT), which uses induced capacitance signal from pairs of capacitance plates surrounding the sensing region to deduce the cross-sectional permittivity distribution of the enclosed space. Since the different phases in a multiphase system tend to possess distinct permittivity constants, the permittivity distribution obtained from ECT can be used to image the multiphase system. The initial development of ECT took place in the 1980 and 1990's where 2-D capacitance tomography was studied for cross-sectional imaging of fluidized bed systems and industrial oil pipelines[12-13]. Later, ECT systems have been widely applied to multiphase flow systems, including gas-solid pneumatic conveying system[14], fluidized bed[15], trickle bed[16], circulating fluidized bed[17], bubble column[18] and so on.

The governing equations for both ECT and ECVT are the same, which is the relation between electrical potential and permittivity distribution:

$$\nabla \cdot \big(\varepsilon(x,y,z)\nabla\varphi(x,y,z)\big) = -\rho(x,y,z) \tag{1.1}$$

where $\varepsilon(x,y,z)$ is the permittivity distribution, $\varphi(x,y,z)$ is the electrical potential distribution which is related to $\varepsilon(x,y,z)$, and $\rho(x,y,z)$ is the charge distribution. Suppose there are n capacitance plates in the ECVT sensor, and the capacitance reading between two of the plates is regarded as one measurement, the total number of independent

capacitance measurements, m, is a 2-combination of n, which equals to $\frac{1}{2}n(n-1)$. Thus, based on Gauss' Law, the capacitance between ith and jth plates C_{ij} is:

$$C_{ij} = \frac{Q}{U_{ij}} = \frac{\oiint \varepsilon \nabla \varphi dA}{U_i - U_j} \tag{1.2}$$

where Q is the electric charge on the excited capacitance plate, U_{ij} is the voltage between the pair of plates, A is the surface unit to be integrated over the capacitance plate surface. To calculate ε from C is difficult because solving the highly non-linear integration equation is hard, and at the same time, the number of known C is limited. To simplify the equation, a linear mapping from ε to C is constructed through sensitivity matrix:

$$C = SG \tag{1.3}$$

where C is the $m\times1$ capacitance vector recording all m independent capacitance response, G is the $k\times1$ image matrix describing the spatial permittivity distribution, and S is the $m\times k$ sensitivity matrix describing the capacitance response to permittivity change in each voxel, and can be obtained in advance by solving the governing equation using finite-element methods. At this stage, solving for G can be done by finding S^T so that:

$$G = S^T C \tag{1.4}$$

However, S^T does not exist because it is an ill-posed problem. At this stage, there are multiple mathematical techniques to solve this problem, including linear back projection (LBP)[19], iterative linear back projection (ILBP)[20], simultaneous image reconstruction technique (SIRT)[21] and neural network multi-criterion optimization technique (NN-MOIRT)[22]. A comparison of the performance of these techniques is shown as follows:

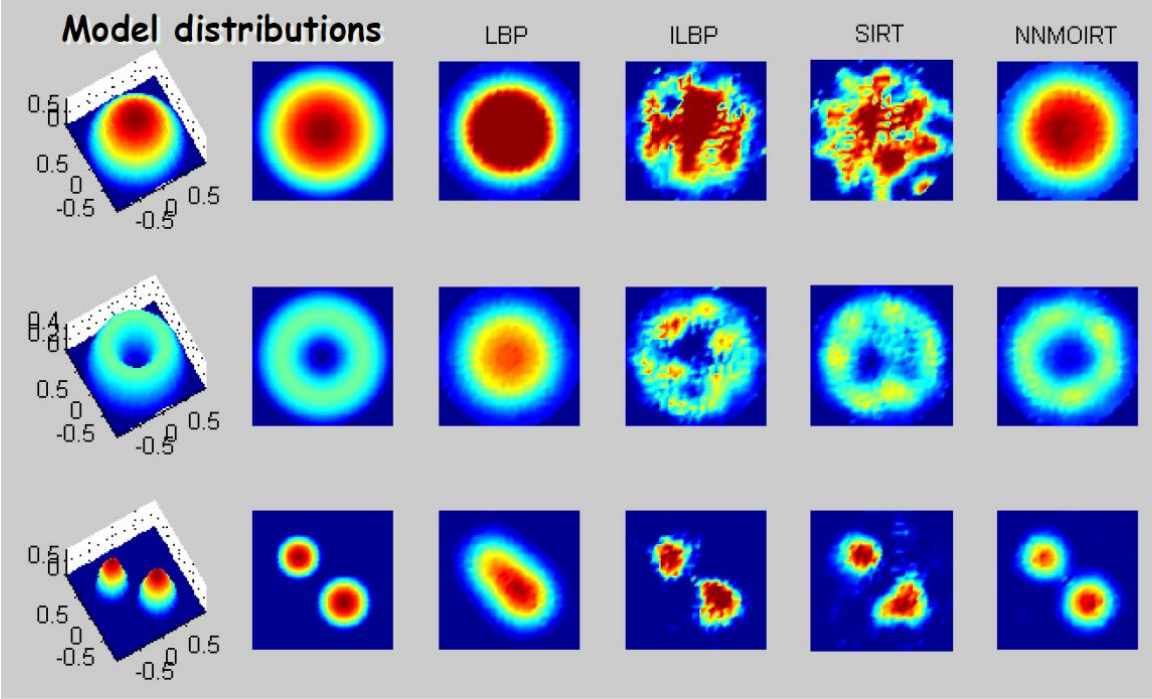

Figure 4. Comparison of the performance of current RCT image reconstruction techniques[18].

1.2.2 Recent developments of ECVT

As a promising imaging technology, ECVT holds its strength in its low cost and fast response in real-time imaging, as well as its flexibility in fitting any type of geometries. To date, ECVT sensors of sizes up to 60' ID have been used in process imaging[1]. Multiphase systems with complex geometries including right-angle exit pipe and tapered column are also investigated using ECVT[23-24]. The high sampling rate of ECVT is also utilized to image fast-speed packed bed flow[25]. 3-D velocity vector fields can also be obtained from ECVT sensors[26]. Up to now, most applications of ECVT are under ambient temperature. The experiment conducted in this work is the first to explore ECVT technology for high-temperature gas-solid fluidized bed system.

1.3 Slugging in Gas-Solid Systems

Slugging is a major fluidization regime typically seen in fluidized beds with large height-to-diameter ratios. In slugging flows, the gas bubble grows to the size of the diameter of the bed. A large height-to-diameter ratio is required for the bubble to grow to the required size, but for coarse or large particles, this ratio can be smaller. Generally, slugging flow can be categorized into round-nosed slug and square-nosed slug based on the shape of the gas slug[27]. Round-nosed slug occurs when fine particles are used, and the particles trickle down along the inner wall of the bed. Square-nosed slug occurs when coarse particles are used and the bed diameter is small. Under such conditions, the particles are prone to bridge, and the particles rain down through the slug. Other types of slug also exist, including

asymmetric slug and wall slug, which can occur when the wall surface is rough, the particle is big relative to the bed, or gas velocity is high.

Generally, the slug rise velocity of an axisymmetric slug can be obtained from:

$$U_{sl} = k_1\left(U_g - U_{mf}\right) + k_2\sqrt{gD} \tag{1.5}$$

where U_{sl} is the slug velocity, U_g is the superficial gas velocity, U_{mf} is the minimum fluidization velocity of the particles, g is the gravitational acceleration and D is the bed diameter. The two coefficients, k_1 and k_2, are experimentally determined to be 1 and 0.35[27].

Experimental characterization of slugging flow is often limited to direct visual observation at ambient temperature for measuring slug velocity, length, frequency due to lack of measurement methods[28]. Pressure measurement is another way of characterizing slugging flow, and slug frequency information can be extracted from pressure fluctuations[29-30].

Chapter 2: Experimental Setup

Generally, ECVT sensors cannot have conductive materials in the sensing region dur to their distortion to the electrical field. Thus, most cold flow studies with ECVT use non-conductive plastic material for the flow vessel, on which ECVT sensor can be directly installed. To allow ECVT sensor to function properly at high temperatures, non-conductive heat-resistant material has to be used to house the sensor. A special ECVT sensor with ceramic lining is designed for this task by Tech4Imaging. The configuration of the whole test system and the experimental procedures are explained below.

2.1 Test Unit Design and Setup

The main component of the high-temperature ECVT test unit is a fluidized bed with 3” ID and 30” height. In the middle of the fluidized bed is the ECVT sensor assembly, which is connected to the stainless-steel reactor columns on both ends. Six 1/4” ID thermocouple ports are positioned along the side of the bed on the two stainless steel sections, and two 1/8’ holes are made on the flanges immediately above and below the sensor assembly for pressure measurements. A 6” ID disengagement section is installed above the bed to prevent solids from being entrained out of the bed at high gas flow rates, which also effectively limits the maximum bed height and minimizes heating power required to maintain high temperatures. The disengagement section is connected to a ceiling fan via a

metal hose, which serves as the gas outlet of the fluidized bed. A gas inlet and particle discharge assembly is installed at the bottom of the bed. Two gas inlet ports are located on opposite sides of the assembly for better gas distribution. A hand valve is used to control particle discharge. The entire fluidized bed assembly is supported by an external framework.

Three sets of 208 V external ceramic heaters are installed on the stainless-steel pipe sections of the bed to supply heat for high-temperature tests. Two air preheaters are installed on the two gas inlets, which also have built-in thermocouples for heater control. The bed and the gas inlets are insulated with ceramic wools to minimize heat loss. The two pressure measurement ports are connected to a differential pressure transducer. The transducer and thermocouples are connected to a process control box, which is connected to a computer in the control room. The heater power is supplied from a relay panel, which is also wired to the process control box for power output control. The air for fluidizing the bed is supplied by an in-house air compressor, and the air flow rate is controlled by a mass flow controller. On the computer in the control room, a human-machine interface is prepared for temperature and pressure recording, heater control and gas flow rate control.

The ECVT sensor has a casted ceramic lining as the inner wall, and a metal shell as the outer casing. 24 capacitance plates are housed inside the cast into 4 levels. The sensor plates are staggered in adjacent layers to improve imaging resolution in the axial direction. The ceramic lining serves both as a non-conductive material that protects the capacitance plate from excess heat, and as a thermal insulation to minimize heat loss in the sensor

section. Each plate has a wire lead for signal collection, and the lead rod is extended all the way to the outside of the ceramic wool insulation on the sensor assembly for easier wiring. Each capacitance plate is wired individually to the data acquisition box, which is then connected to the computer in the control room. Photographs of the ECVT test unit and an illustration of the system are shown as follows:

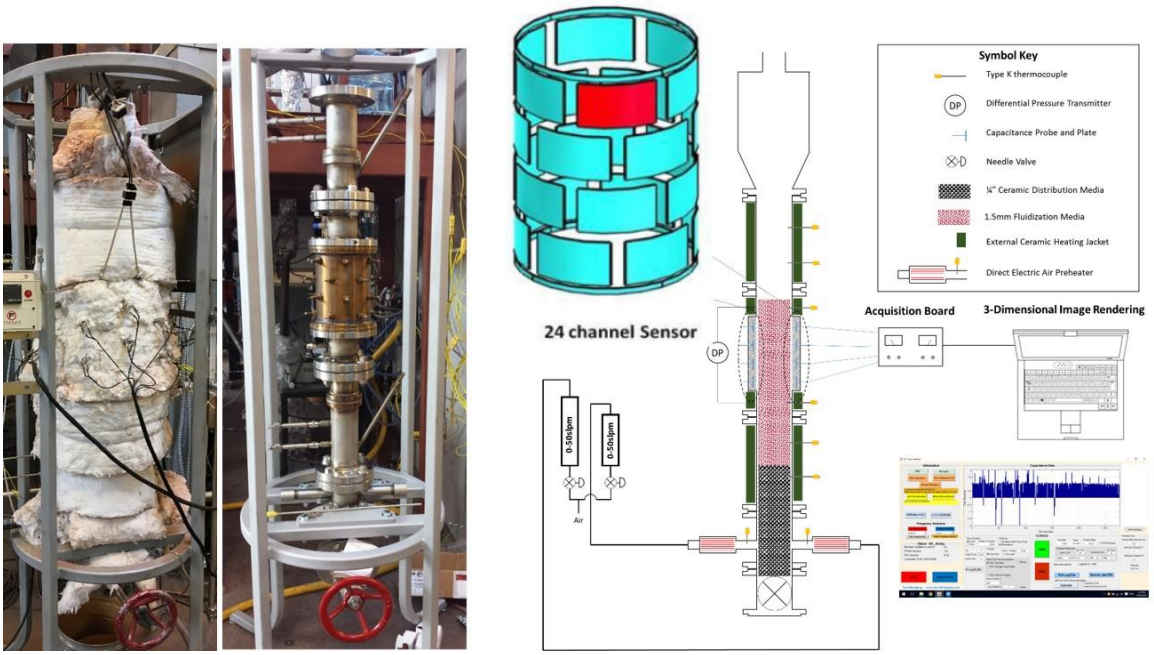

Figure 5. Photographs of the test unit with and without insulation (left) and illustration of the ECVT sensor and test unit design (right).

2.2 Experimental Procedures

At the start of each experiment, the ECVT system needs to be calibrated and normalized. For calibration, the driver amplitude of the excitation signal from sensor plates is determined by taking measurements of the empty and full bed, where empty means the bed is empty with only air inside, and full means the bed is filled with packed, stationary solids to a level at least above the sensing region. This ensures a maximum digital quantization resolution while also ensuring no information is lost due to clipping. The signal balance of the sensor plates is then determined by offsetting the signal phase until the received signal matches the transmitted signal during data collection from the empty sensor region. This is to make sure that the ceramic lining no longer contributes to the change in signal from excite to receive plates. For normalization, the measurements are taken once again from both empty and full bed, and the data is used to normalize the maximum signal amplitude, which corresponds to the full bed condition, and the minimum signal amplitude, which corresponds to the empty bed condition, to 1 and 0. This is to simplify capacitance measurements and will facilitate data processing and image reconstruction in the software.

After sensor calibration and normalization, the unit is ready for slugging fluidization characterizations. The two control variables in the fluidization tests are inlet air flow rate and temperature, and the behavior of the fluidized bed is recorded by ECVT at various test conditions. The range of air flow rates is chosen such that the bed evolves from minimum fluidization condition to slugging fluidized bed condition, but not to entrainment condition.

Chapter 3: Results and Discussion

A series of slugging fluidized bed tests are conducted in the high-temperature test unit, covering different flow rates at temperatures ranging from room temperature to 700 °C. The superficial gas velocity ranges from 0.25 m/s to 2 m/s over the minimum fluidization velocity of the particles under the respective temperatures to maintain the slugging flow regime without causing entrainment. As the experiments progress, several operational issues with the test unit and ECVT image reconstruction performance issues are identified and addressed. After the system's performance is optimized, extensive testing is conducted repeatedly to validate the consistency of the data. Slugging fluidized bed behaviors obtained from the ECVT are also validated with pressure drop measurements.

The reconstructed 3-D images of the slugging fluidized bed essentially provide time-dependent spatial solids holdup distribution in the sensing region, from which the slug velocity and frequency data can be extracted through cross-correlation of the solids holdup profiles at different heights and spectrum analysis of the solids holdup profiles. The obtained correlations between these two slug properties and superficial gas velocity are compared with literature data, and the effect of temperature is discussed.

In the end, the conclusion is reached that using ECVT at high temperature is feasible. Plans for improving the performance of ECVT at high temperatures and for employing ECVT for solids circulation rate measurement in the chemical looping system are also proposed.

3.1 Performance Optimization of the Test Unit

3.1.1 Temperature Uniformity Optimization

Temperature uniformity is crucial in gas-solid fluidization systems because the physical properties of the gas, including gas density and viscosity, change as temperature changes, which also cause the gas velocity to change even when the inlet flow rate is kept the same. These changes affect the force between gas and solid, solid and solid, and solid and reactor wall, which altogether determine the fluidization behavior of the bed. If the temperature is not uniform in the bed, these properties will not be uniform either, which causes deviation from ideal theoretical conditions and significantly complicates the experiments for parametric studies. Generally, in a fluidized bed reactor comparable to the size of the high-temperature ECVT test unit, temperature uniformity at high temperatures is achievable with external heaters completely covering the entire length of the bed. At the same time, fluidization also enhances heat transfer in the bed and helps distribute temperature evenly. However, in the high-temperature ECVT unit, the sensor assembly does not have external heaters, because the sensor plates and built-in electrical connections are vulnerable to high temperatures. Due to the lack of external heaters in this region, the heat loss is greater compared to the heated sections above and below the sensing region.

Initial testing shows that when the bed is heated up in a packed bed configuration, only the temperatures in the heated section increase, and when the temperature reaches the desired set point, as soon as the fluidization gas is introduced, the temperature of the bed starts to drop. The reconstructed image from these tests are found to be of low quality. To solve this issue, the bed is kept at fluidized condition during heat up. This would help bring heat to the unheated sensing region, and improve the temperature uniformity throughout the reactor. After this method is implemented, the temperature difference of the bed can be maintained well within 100 °C, as is shown in the following plot from a representative experiment at 700 °C. Note that the jump changes in temperature is caused by the changes in inlet air flow rate.

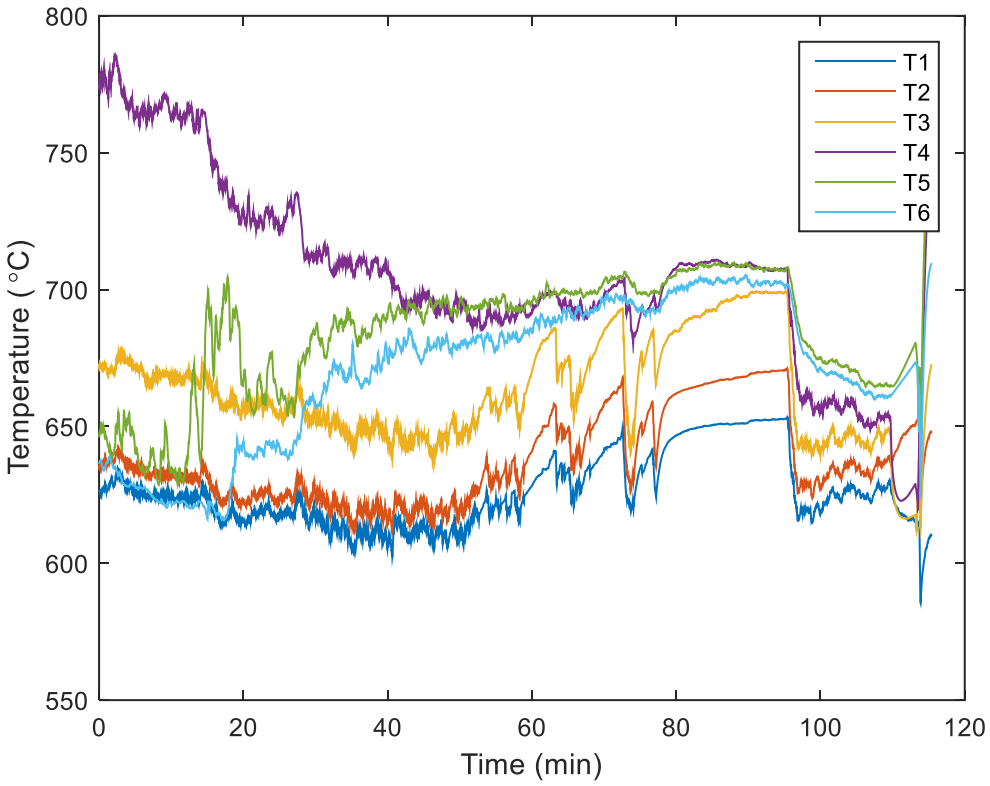

Figure 6. Temperature profile of the fluidized bed during an experiment at 700 °C, where T1 ~ T6 refer to the thermocouples on the side of the bed, from top to bottom.

3.1.2 ECVT Performance Optimization

During several preliminary tests, the signal-to-noise ratios of certain channels of the ECVT sensor are found to be high, which is reflected by constant fluctuations in the capacitance reading of the respective channels. To solve this issue, the standard deviations of the capacitance readings from the channels over a period of 20 s is calculated, which reflects the signal-to-noise ratios of the respective channels. A representative example of the deviation data is shown as follows:

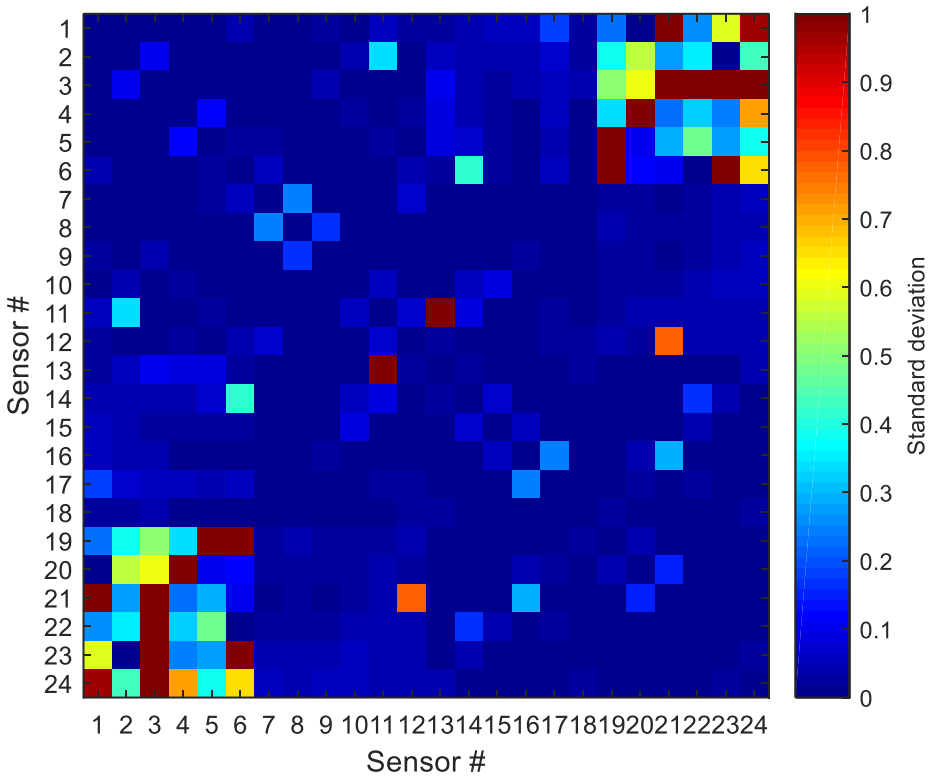

Figure 7. Standard deviations of the normalized capacitance signals from all 276 channels in an empty bed at room temperature in one experiment.

In the matrix above, each box represents the channel formed by the corresponding pair of sensor plates. Note that the standard deviations of some channels exceeded 1 but are scaled down to 1 in the figure for better representation. It can be seen that the standard deviations of the channels corresponding to sensor plate 1~6 against 19~24 are significantly higher than those of other channels, which implies that the quality of the signals measured between the top plates and the bottom plates are subpar to the rest of the channels, which are from the plates in the same or adjacent layers. This is to be expected because the distance between the top and bottom plates are longer, which weakens the capacitance signal, thus lowering the signal-to-noise ratio. Initially, without any data pre-processing, the 3-D images reconstructed from these data that contain high signal-to-noise ratio channels tend to have distortions and artifacts, which hinders the capture of the actual flow conditions in the fluidized bed. This issue is solved by ignoring these "noisy" channels when executing the image reconstruction algorithm, which eliminates interference from these channels only at the cost of slightly decreasing the image resolution.

3.1.3 ECVT Performance Validation with Pressure Drop Measurements

After the temperature uniformity and image reconstruction issues are solved, the ECVT performance is evaluated by comparing the overall solids holdup calculated from reconstructed ECVT images to the solids holdup obtained from pressure drop across the sensing region. In a fluidized bed, the solids holdup across a certain region refers to the volume fraction of the solids within the defined region, which is proportional to its pressure drop. A fluctuation in the holdup in a slugging bed corresponds to the passing of the slug

through the region. When the solid plug passes through, a high solids holdup is registered, whereas when a gas slug is passing through, a low solids holdup is registered. Note that the solids holdup can be directly obtained from the reconstructed image from ECVT since it contains the spatial distribution of the solids fraction, and in most cases can be directly obtained from pressure drop too since it is approximately proportional to the weight of the solids. However, the solids holdup cannot be directly obtained from the pressure drop in a slugging bed because wall friction also contributes significantly to the pressure drop. Thus, the solids holdup profile from ECVT is superimposed on the pressure drop profile after normalization, such that only the pattern of fluctuation is left for comparison. The results from two representative conditions are shown as follows:

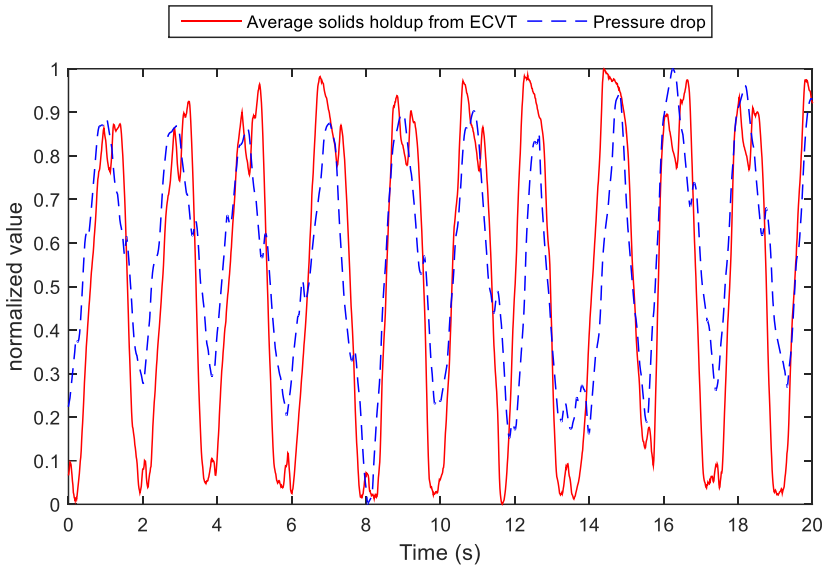

(a) Ambient temperature with superficial gas velocity of 0.67 m/s

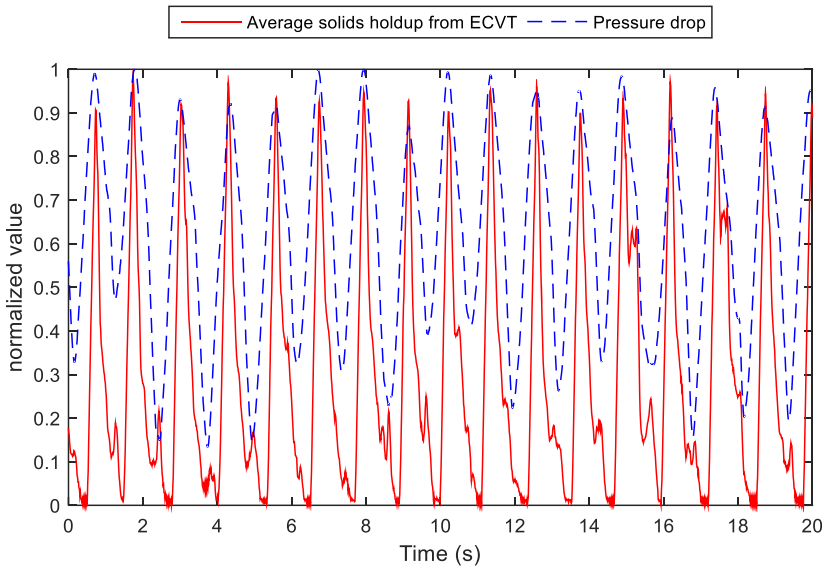

(b) 400 °C temperature with superficial gas velocity of 1.7 m/s

Figure 8. Comparison of solids holdup from ECVT with that from pressure drop.

It can be seen that solids holdup profile from ECVT matches pressure drop profile from the differential pressure transducer, which indicates that the dynamic slugging behaviors obtained from ECVT, including slug duration and slug frequency, is consistent with those from the pressure drop. It can also be seen that temperature and flow rate does not affect the fidelity of ECVT measurements.

3.2 Slug Velocity and Frequency

3.2.1 Slug Velocity vs. Gas Flow Rate

To calculate the slug velocity, average solids holdup across each horizontal plane in the sensing region is first obtained. As slug passes through the sensing region, the solids holdup for each horizontal plane periodically increases then decreases, forming a wave-like pattern in the solids holdup profile. Depending on the height of the plane, the peak generated from the same slug occurs at slightly different times on different planes. Using cross-correlation, the lag between the solids holdup profiles at different heights can be found, which corresponds to the time required for the slug to travel the respective height difference, from which the slug velocity can be derived. An illustration of this process is shown as follows:

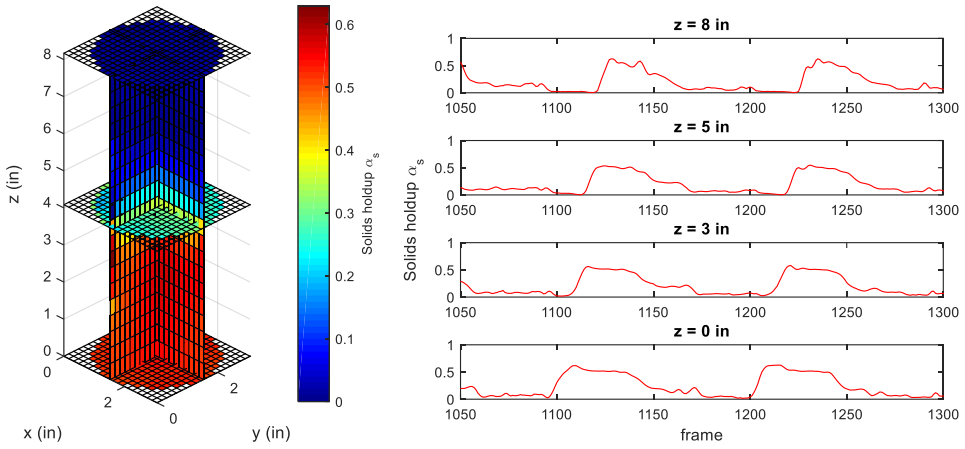

(a) Reconstructed image (left) and the staggering of solids holdup profiles at different heights (right)

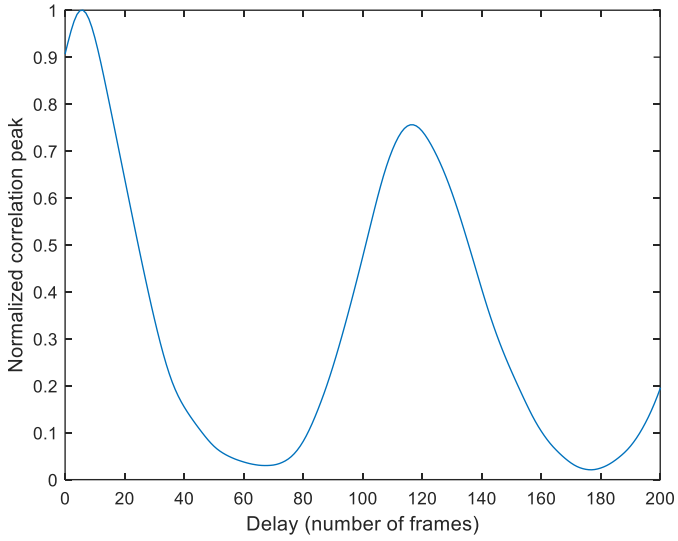

(b) Cross-correlation between solids holdup profiles from z = 5'' and z = 3''

Figure 9. Illustration of the process for calculating slug velocity (data from 23 °C, U - U_{mf} = 1.81 m/s) .

According to the two-phase theory, the slug velocity is proportional to the difference between superficial gas velocity and the minimum fluidization velocity. The results from the experiments at different temperatures are shown as follows:

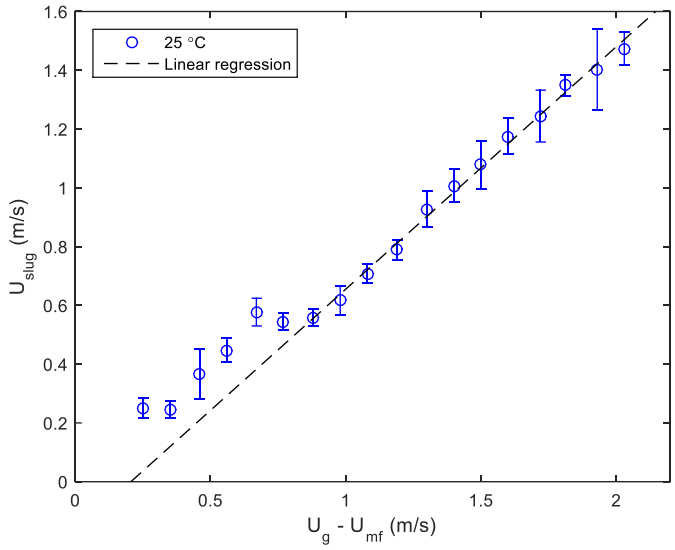

(a)

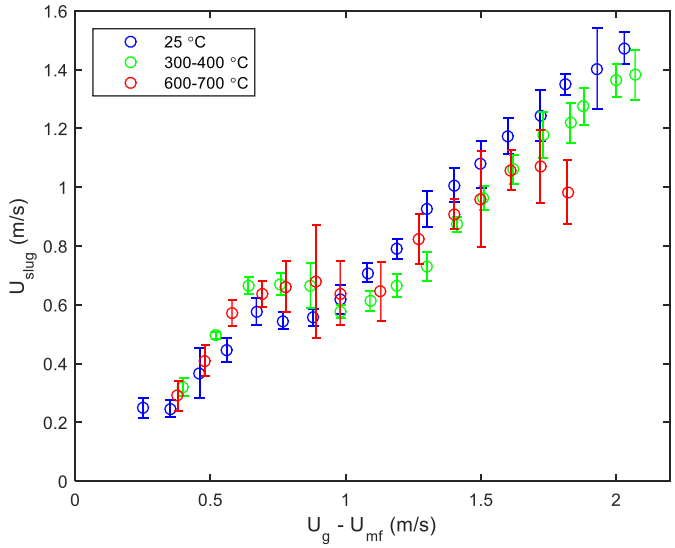

(b)

Figure 10. Slug velocity vs. superficial gas velocity minus minimum fluidization velocity at (a) room temperature and (b) all the temperatures tested.

Note that in the figures above, the error bar represents the standard deviation of the results from multiple repeated experiments at each gas flow rate. It can be seen that the slug velocity increases linearly beyond certain point with respect to the superficial gas velocity, which is consistent with the two-phase theory and literature data[27, 31-32]. The data at low gas velocities does not match the linear trend, because the bed is still in the bubbling regime under those conditions. The turning point from the bubbling regime to the fully developed slugging regime, where the slug velocity decreases after the initial increase, is called the onset of slugging[32]. However, the values of parameters for the regression line, namely $k_1 = 0.553$ and $k_2 = 0.032$, are different from literature values[27], where $k_1 = 1$ and $k_2 = 0.35$. This is due to the fact that the literature values are obtained for round-nosed slug, which is different from the square-nosed slug formed in the ECVT test unit. For square-nosed slugs, the solids are closer to a bridging state rather than a fluidized emulsion phase, which may cause the parameters to be lower than those with round-nosed slugs. As for temperature, its effect on the slug velocity for the iron oxide particles tested are not pronounced since the slug velocity profiles obtained at high temperatures do not deviate significantly from the one at room temperature.

3.2.2 Slug Frequency vs. Gas Flow Rate

The solids holdup profiles obtained for slug velocity calculations can be directly used to obtain slug frequency by conducting a spectral analysis. Each peak in the profile corresponds to a slug, thus, the frequency of the peak is equivalent to slug frequency. The frequency is calculated by performing fast Fourier transform on the solids holdup profiles

and identifying the dominant frequency in the frequency domain. An example of the process is shown as follows:

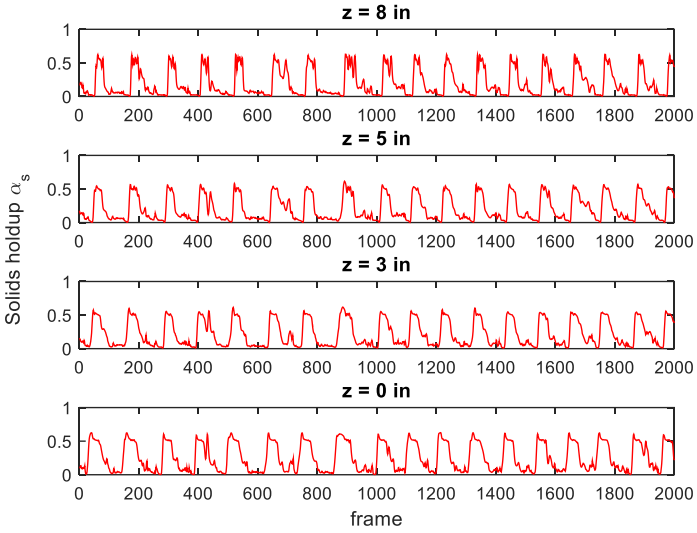

(a) Solids holdup profiles at different heights

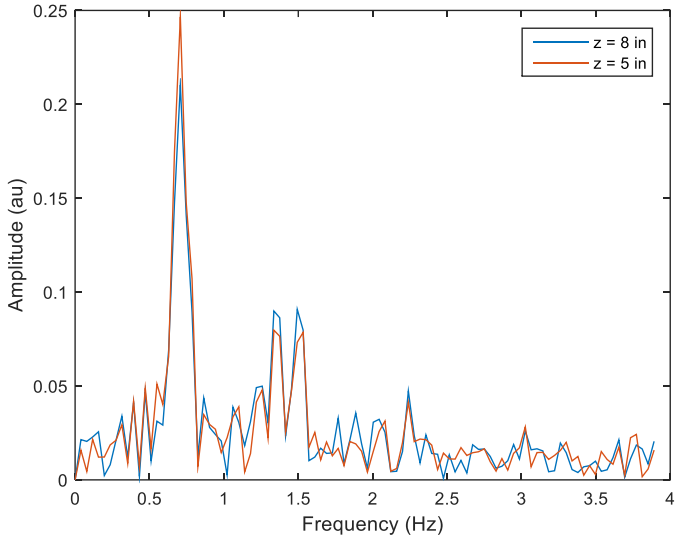

(b) Frequency domains of the solids holdup profiles at z = 5'' and z = 8''

Figure 11. Illustration of the process for calculating slug frequency (data from 23 °C, U - U_{mf} = 1.81 m/s) .

The results from the experiments at different temperatures are shown as follows:

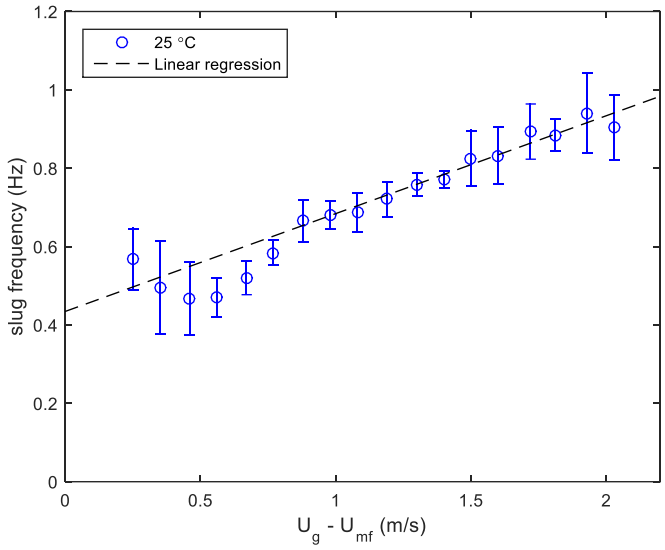

(a)

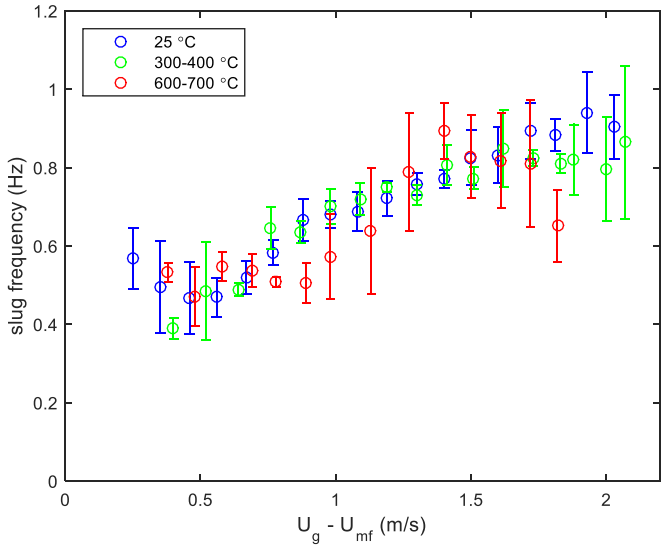

(b)

Figure 12. Slug frequency vs. superficial gas velocity minus minimum fluidization velocity at (a) room temperature (frequency is translated to time interval between adjacent slugs for easier understanding) and (b) all the temperatures tested.

Note that in the figures above, the error bar represents the standard deviation of the results from multiple repeated experiments at each gas flow rate. It can be seen that in the fully developed slugging regime, the slug frequency gradually increases as gas velocity increase, until the frequency reaches about 1 Hz. This is inconsistent with literature data, where the slug frequency decreases with increasing gas velocity[29, 31]. This is possibly due to the added disengagement section in the high-temperature ECVT setup, where solid slug collapses immediately after entering the disengagement zone, thus limiting the travel distance of the slug, and causing the frequency to increase as velocity increases, whereas in the experiments reported in literature, solid slugs can travel upwards freely until it reaches maximum bed height, thus the travel distance of the solid slug increases, which negates the effect of the increase in velocity on frequency. As for temperature, its effect on the slug frequencies are not pronounced since the slug frequency profiles obtained at high temperatures do not deviate significantly from the one at room temperature.

3.2.3 Interpreting Reconstructed Images

The reconstructed images help visualize the slugging behavior in the test unit, which can greatly facilitate the viewer to monitor slugging fluidized beds in real-world applications. The following reconstructed images are side views of the sensing region under different temperature and gas flow rate conditions:

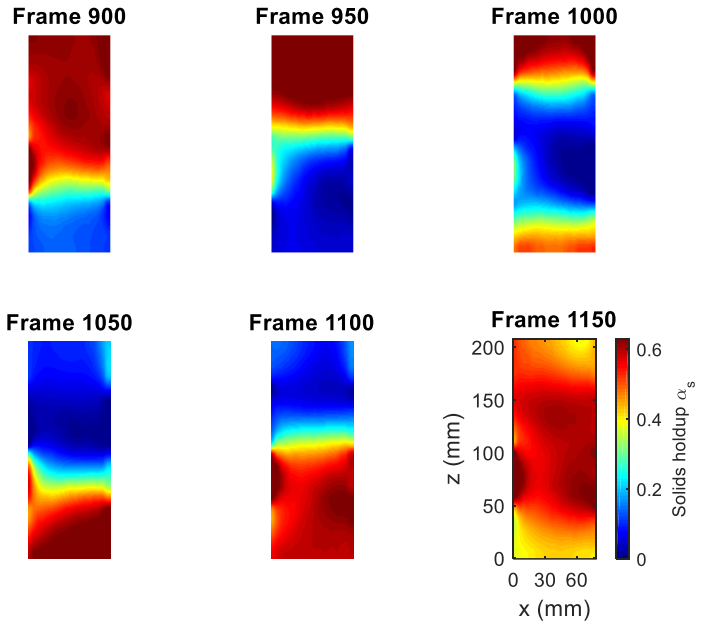

(a) Reconstructed slug images (310 °C, U - U_{mf} = 0.44 m/s, time interval 0.19 s)

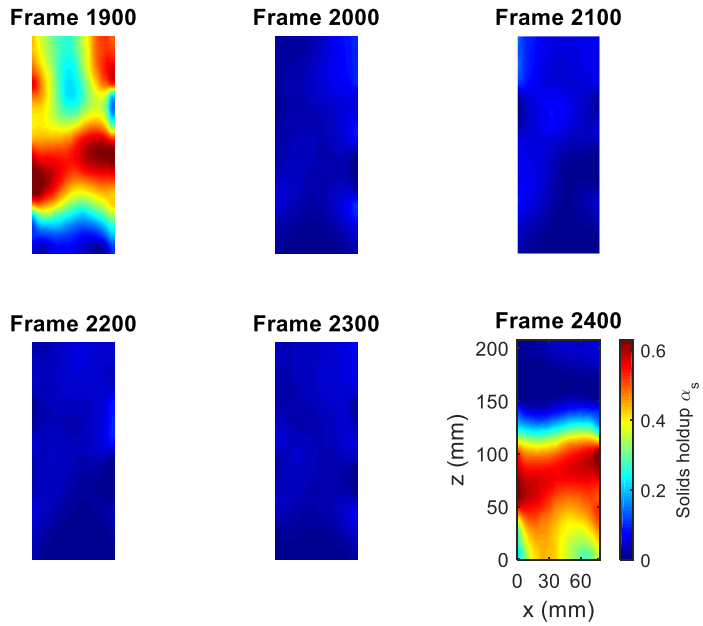

(b) Reconstructed slug images (610 °C, U - U_{mf} = 1.81 m/s, time interval: 0.38 s)

Figure 13. Side view of the sensing region showing solids holdup data.

It can be seen that in the first condition, it takes longer time for the slug to pass through the sensing region, whereas in the second condition, it takes shorter time. This is a direct reflection of the difference in slug velocity under these two conditions.

The difference between the bubbling regime when the gas velocity is low and the fully developed slugging regime when the gas velocity is high is also evidently shown in the reconstructed images, as are shown below:

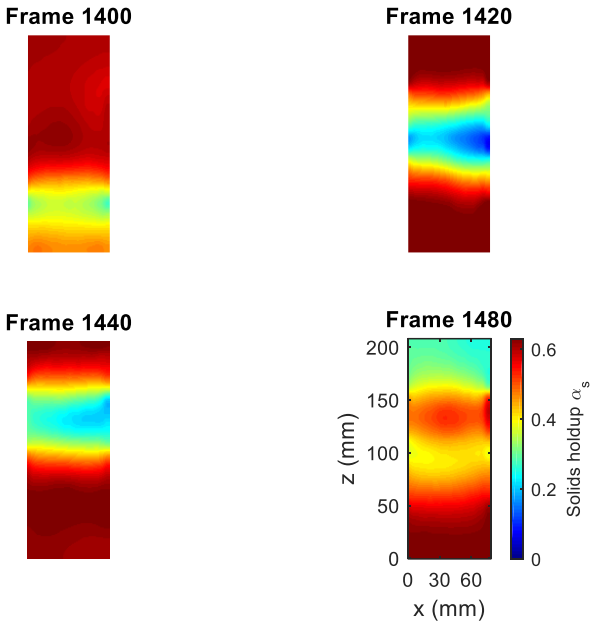

(a) Evolution of a non-slug signal (ambient temperature, U_g - U_{mf} = 0.25 m/s)

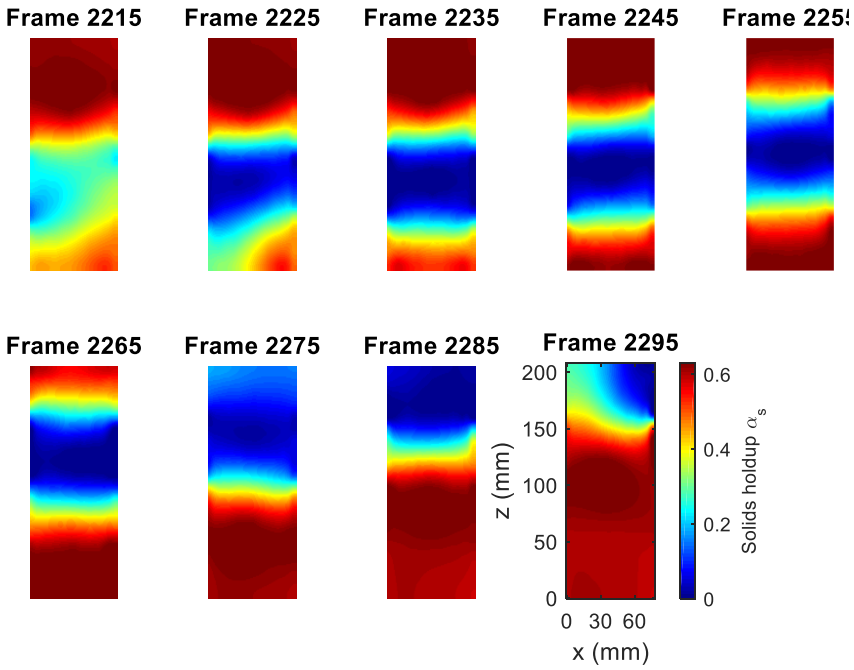

(b) Evolution of a slug (ambient temperature, U_g - U_{mf} = 0.41 m/s)

Figure 14. Comparison between non-slug and slug regimes.

It can be seen that under the first condition, the dilute region, which usually represents a gas bubble, still has a high solids holdup, which indicates that the two adjacent solid slugs are not completely separated. Whereas under the second condition, the dilute region barely has any solids holdup, which indicates the gas slug is fully developed.

3.3 Conclusion and Future Plans

The experiments performed in this work proves that ECVT imaging technology can be applied to high-temperature gas-solid fluidization systems. Specifically, a slugging fluidized bed configuration with Geldart Group D particles is studied, and the correlations between slug velocity/frequency and gas velocity are established at temperatures ranging from ambient to 700 °C. It is found that as gas velocity increases, slug velocity increases linearly, and slug frequency increases as well, but approaches 1 Hz in the end. Temperature is found to have little effect on the correlations. The linearity in the correlations is consistent with the two-phase theory, but the coefficients are different from literature values.

The plan for the ECVT test unit is to extend the fluidized bed test to more types of particles at high temperatures. This not only would acquire room temperature data over a wide range of solids that can be compared with literature data, but also explore the temperature effect on them.

For the application in chemical looping systems, the current test unit will be modified so that it can test moving bed solids velocity. A preliminary test in done by discharging a packed bed in the test unit and taking ECVT measurements. The velocity can be obtained from the cross-correlation of the raw capacitance reading from adjacent channels, as is shown below:

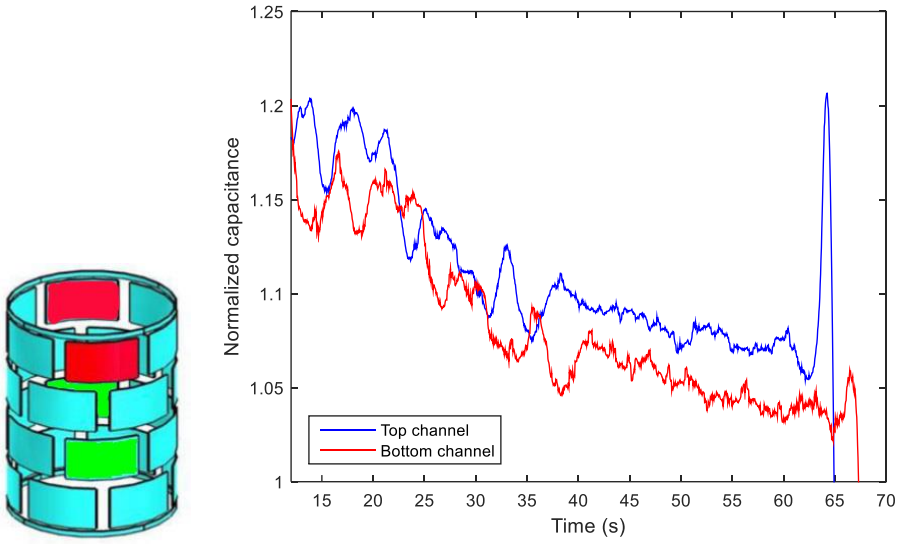

Figure 15. Adjacent channels in the ECVT sensor (left) and the corresponding raw capacitance readings (right) as the bed is descharged.

Finite element method will also be explored to help with the ECVT calibration and normalization procedures. Designing an ECVT sensor assembly for the in-house chemical looping sub-pilot unit is also needed to be able to test its ability to measure solids circulation rate at high temperature in real world.

References

1. Wang, F.; Marashdeh, Q.; Fan, L. S.; Warsito, W., Electrical capacitance volume tomography: design and applications. *Sensors (Basel)* **2010,** *10* (3), 1890-917.

2. U.S. Energy Information Administration, International Energy Outlook 2016.

3. U.S. Energy Information Administration, Annual Energy Outlook 2017.

4. Rubin, E. S.; Chen, C.; Rao, A. B., Cost and performance of fossil fuel power plants with CO2 capture and storage. *Energy Policy* **2007,** *35* (9), 4444-4454.

5. Boot-Handford, M. E.; Abanades, J. C.; Anthony, E. J.; Blunt, M. J.; Brandani, S.; Mac Dowell, N.; Fernández, J. R.; Ferrari, M.-C.; Gross, R.; Hallett, J. P.; Haszeldine, R. S.; Heptonstall, P.; Lyngfelt, A.; Makuch, Z.; Mangano, E.; Porter, R. T. J.; Pourkashanian, M.; Rochelle, G. T.; Shah, N.; Yao, J. G.; Fennell, P. S., Carbon capture and storage update. *Energy Environ. Sci.* **2014,** *7* (1), 130-189.

6. Wang, M.; Lawal, A.; Stephenson, P.; Sidders, J.; Ramshaw, C., Post-combustion CO2 capture with chemical absorption: A state-of-the-art review. *Chemical Engineering Research and Design* **2011,** *89* (9), 1609-1624.

7. Scheffknecht, G.; Al-Makhadmeh, L.; Schnell, U.; Maier, J., Oxy-fuel coal combustion—A review of the current state-of-the-art. *International Journal of Greenhouse Gas Control* **2011,** *5*, S16-S35.

8. Fan, L.-S.; Zeng, L.; Luo, S., Chemical-looping technology platform. *AIChE Journal* **2015,** *61* (1), 2-22.

9. Li, F.; Zeng, L.; Velazquez-Vargas, L. G.; Yoscovits, Z.; Fan, L.-S., Syngas chemical looping gasification process: Bench-scale studies and reactor simulations. *AIChE Journal* **2010,** *56* (8), 2186-2199.

10. Fan, L. S., Metal Oxide Reaction Engineering and Particle Technology Science: A Gateway to Novel Energy Conversion Systems. *The American Institute of Chemical Engineers (AIChE) 67th Institute Lecture* **2015**.

11. Luo, S.; Zeng, L.; Xu, D.; Kathe, M.; Chung, E.; Deshpande, N.; Qin, L.; Majumder, A.; Hsieh, T.-L.; Tong, A.; Sun, Z.; Fan, L.-S., Shale gas-to-syngas chemical looping process for stable shale gas conversion to high purity syngas with a H2 : CO ratio of 2 : 1. *Energy Environ. Sci.* **2014,** *7* (12), 4104-4117.

12. Beck, M. S.; Morris, M., *Tomographic Techniques for Process Design and Operation*. Computational Mechanics Publ.: 1993.

13. Fashching, G. E.; Smith, N. S., *High resolution capacitance imaging system: Technical note*; DOE/METC-88/4083; Other: ON: DE88010277 United States Other: ON: DE88010277 NTIS, PC A03/MF A01 - OSTI; 1. TIC English; ; USDOE Morgantown Energy Technology Center, WV: 1988; p Medium: X; Size: Pages: 44.

14. Dyakowski, T.; Luke, S. P.; Ostrowski, K. L.; Williams, R. A., On-line monitoring of dense phase flow using real time dielectric imaging. *Powder Technology* **1999,** *104* (3), 287-295.

15. Dyakowski, T.; Edwards, R. B.; Xie, C. G.; Williams, R. A., Application of capacitance tomography to gas-solid flows. *Chemical Engineering Science* **1997,** *52* (13), 2099-2110.

16. Reinecke, N.; Mewes, D., Investigation of the two-phase flow in trickle-bed reactors using capacitance tomography. *Chemical Engineering Science* **1997,** *52* (13), 2111-2127.

17. Srivastava, A.; Agrawal, K.; Sundaresan, S.; Reddy Karri, S. B.; Knowlton, T. M., Dynamics of gas-particle flow in circulating fluidized beds. *Powder Technology* **1998,** *100* (2-3), 173-182.

18. Warsito, W.; Fan, L. S., Measurement of real-time flow structures in gas–liquid and gas–liquid–solid flow systems using electrical capacitance tomography (ECT). *Chemical Engineering Science* **2001,** *56* (21-22), 6455-6462.

19. Peng, L.; Merkus, H.; Scarlett, B., Using Regularization Methods for Image Reconstruction of Electrical Capacitance Tomography. *Particle & Particle Systems Characterization* **2000,** *17* (3), 96-104.

20. Yang, W. Q.; Spink, D. M.; York, T. A.; McCann, H., An image-reconstruction algorithm based on Landweber's iteration method for electrical-capacitance tomography. *Measurement Science and Technology* **1999,** *10* (11), 1065-1069.

21. Bangliang, S., The use of simultaneous iterative reconstruction technique for electrical capacitance tomography. *Chemical Engineering Journal* **2000,** *77* (1-2), 37-41.

22. Warsito, W.; Fan, L. S., Neural network based multi-criterion optimization image reconstruction technique for imaging two- and three-phase flow systems using electrical capacitance tomography. *Measurement Science and Technology* **2001,** *12* (12), 2198-2210.

23. Wang, F.; Marashdeh, Q.; Wang, A.; Fan, L.-S., Electrical Capacitance Volume Tomography Imaging of Three-Dimensional Flow Structures and Solids Concentration Distributions in a Riser and a Bend of a Gas–Solid Circulating Fluidized Bed. *Industrial & Engineering Chemistry Research* **2012,** *51* (33), 10968-10976.

24. Wang, A.; Marashdeh, Q.; Fan, L.-S., ECVT imaging of 3D spiral bubble plume structures in gas-liquid bubble columns. *The Canadian Journal of Chemical Engineering* **2014,** *92* (12), 2078-2087.

25. Wang, A.; Marashdeh, Q.; Motil, B. J.; Fan, L.-S., Electrical capacitance volume tomography for imaging of pulsating flows in a trickle bed. *Chemical Engineering Science* **2014,** *119*, 77-87.

26. Chowdhury, S.; Marashdeh, Q. M.; Teixeira, F. L., Velocity Profiling of Multiphase Flows Using Capacitive Sensor Sensitivity Gradient. *IEEE Sensors Journal* **2016**, 1-1.

27. Stewart, P. S. B.; Davidson, J. F., Slug flow in fluidised beds. *Powder Technology* **1967,** *1* (2), 61-80.

28. Thiel, W. J.; Potter, O. E., Slugging in Fluidized Beds. *Industrial & Engineering Chemistry Fundamentals* **1977,** *16* (2), 242-247.

29. Noordergraaf, I. W.; Van Dijk, A.; Van Den Bleek, C. M., Fluidization and slugging in large-particle systems. *Powder Technology* **1987,** *52* (1), 59-68.

30. Cho, H.; Han, G.; Ahn, G., Characteristics of slug flow in a fluidized bed of polyethylene particles. *Korean Journal of Chemical Engineering* **2002,** *19* (1), 183-189.

31. Satija, S.; Fan, L.-S., Characteristics of slugging regime and transition to turbulent regime for fluidized beds of large coarse particles. *AIChE Journal* **1985,** *31* (9), 1554-1562.

32. Fan, L. T.; Ho, T.-C.; Walawender, W. P., Measurements of the rise velocities of bubbles, slugs and pressure waves in a gas-solid fluidized bed using pressure fluctuation signals. *AIChE Journal* **1983,** *29* (1), 33-39.